Journal of Power Sources 218 (2012) 6–14

Contents lists available at SciVerse ScienceDirect

Journal of Power Sources

journal homepage: www.elsevier.com/locate/jpowsour

Fracture and debonding in lithium-ion batteries with electrodes of hollow core–shell nanostructures

Kejie Zhao, Matt Pharr, Lauren Hartle, Joost J. Vlassak, Zhigang Suo*

School of Engineering and Applied Sciences, Harvard University, Cambridge, MA 02138, USA

HIGHLIGHTS

- We identify two critical failure modes in a coated-hollow electrode particle.
- We calculate the stress fields in spherical and cylindrical nanostructures.
- We present conditions to avert fracture and debonding.
- We discuss the stress effect on the lithiation reaction.

ARTICLE INFO

Article history:
Received 21 April 2012
Received in revised form
18 June 2012
Accepted 21 June 2012
Available online 28 June 2012

Keywords:
Lithium-ion batteries
Fracture
Debonding
Silicon

ABSTRACT

In a novel design of lithium-ion batteries, hollow electrode particles coated with stiff shells are used to mitigate mechanical and chemical degradation. In particular, silicon anodes of such core–shell nanostructures have been cycled thousands of times with little capacity fading. To reduce weight and to facilitate lithium diffusion, the shell should be thin. However, to avert fracture and debonding from the core, the shell must be sufficiently thick. This tradeoff is considered here by calculating the stress fields resulting from concurrent insertion reaction and plastic flow for both spherical and cylindrical hollow core–shell nanostructures. Conditions to avert fracture and debonding are identified in terms of the radius of the core, the thickness of the shell, and the state of charge. The effect of the stress on the electrochemical reaction is also discussed.

1. Introduction

High capacity lithium-ion batteries are ubiquitous in portable electronics. Development of these batteries is further motivated by their potential use in electric vehicles [1,2]. Silicon can host a large amount of lithium, making it one of the most promising materials to replace the conventional carbon-based anodes [3]. The commercialization of silicon anodes is mainly limited by mechanical failure and chemical degradation [4,5]. Mechanical failure results from the dramatic swelling and stress generated during cyclic lithiation and delithiation. The stress may cause fracture of the conductive matrix and active particles, leading to the loss of the conduction path for electrons, Fig. 1(a). As a result, rapid capacity fading of silicon often occurs in the first few cycles [6,7]. Chemical degradation is attributed mainly to the formation of solid electrolyte interphase (SEI) resulting from the reactions between the electrode and the electrolyte [5]. The formation of the SEI consumes active materials and results in irreversible capacity loss in the first cycle, Fig. 1(b). Furthermore, the repeated swelling and deswelling can cause continual shedding and re-forming of the SEI during cycling, resulting in a persistent decrease in the long-term coulombic efficiency [4].

Recent experiments show that mechanical failure can be mitigated by using nanostructured silicon anodes, such as nanowires [8], thin films [9–12], hollow nanoparticles [13], and nanoporous structures [14]. These structures alleviate the stress by managing the deformation through shape optimization and geometric restrictions [15]. Furthermore, intense efforts are being dedicated to stabilizing the SEI layer during lithiation cycles. Current methods include coating a thin artificial SEI layer on the surface of silicon [15–21] and using electrolyte additives to avoid the continual consumption of active materials [22–27].

A recent design of electrodes involves hollow core–shell nanostructures, which can enhance the mechanical and chemical stability of silicon anodes simultaneously, Fig. 1(c). Such structures

* Corresponding author. Tel.: +1 617 495 3789; fax: +1 617 296 0601.
E-mail address: suo@seas.harvard.edu (Z. Suo).

0378-7753/$ – see front matter © 2012 Elsevier B.V. All rights reserved.
http://dx.doi.org/10.1016/j.jpowsour.2012.06.074

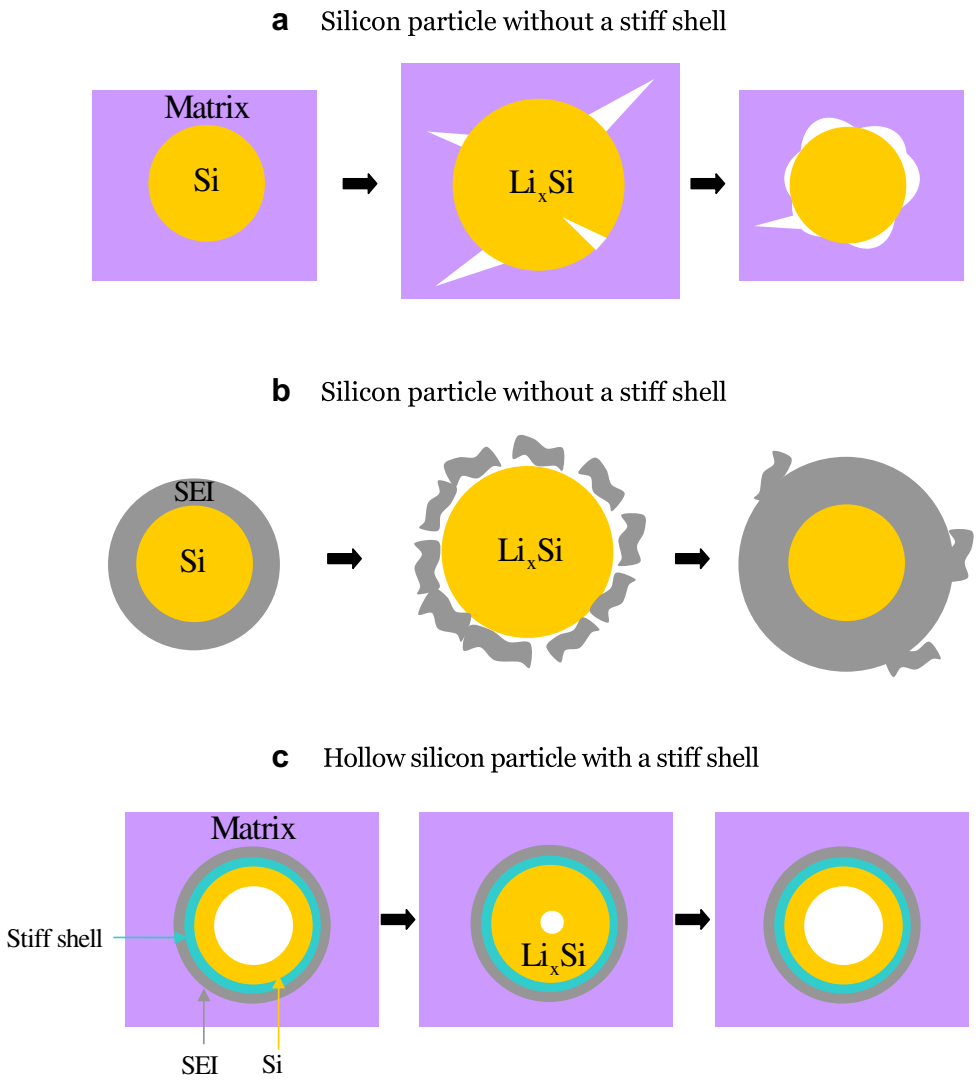

Fig. 1. (a). For a silicon particle without a stiff shell, the stress induced by lithiation and delithiation may cause fracture of the active particle, or debonding between the active particle and the matrix, leading to the loss of the conduction path for electrons. (b). Also for a silicon particle without a stiff shell, the deformation associated with lithiation and delithiation may cause the shedding and re-forming of the solid-electrolyte interphase (SEI), consuming active materials. (c). For a hollow silicon particle with a stiff shell, the deformation of silicon is accommodated by inward swelling, so that electric contact is maintained, and the shedding of SEI avoided.

enable silicon electrodes to sustain over six thousand cycles with high coulombic efficiency [28]. In a hollow core–shell nanostructure, the shell separates the electrolyte and the electrode (core), and forces the core to swell into the hollow space in the interior of the structure. Because the shell restricts outward swelling of the core, the continual SEI shedding and re-forming is suppressed, and the electric contact between the electrode and the matrix is maintained. Similar designs based on encapsulating silicon nanoparticles within hollow carbon shells show promise for high-capacity electrodes with long cycle life of hundreds of cycles [29–31].

Constrained lithiation and delithiation, however, induce stress in the hollow core–shell structures. During lithiation, Fig. 2(a), the core is under compressive stresses, and the shell is under tensile hoop stress. Such tensile stress can initiate fracture in the shell. During delithiation, Fig. 2(b), the radial stress can be tensile in both the core and the shell. Such stress may cause interfacial debonding. To facilitate lithium diffusion and reduce overall weight, the ideal stiff shell should be thin. However, an extremely thin shell is unable to constrain the outward expansion of the core. The insertion reaction causes large deformation in the core, but the magnitude of the stress is kept manageable by plastic flow. Here we calculate the stress field resulting from the concurrent insertion reaction and plastic flow in hollow spherical nanoparticles and nanowires of silicon coated with stiff shells. We identify conditions to avoid fracture and debonding in terms of the radius of the core, the thickness of the shell, and the state of charge. We further identify the driving forces for the lithiation reaction and discuss the effect of the stress field on the electrochemical reaction.

2. Stresses in coated hollow spherical particles of silicon

In a hollow core–shell structure, the stiff shell forces the core to swell into the inner hollow space (Fig. 3). Before absorbing any lithium, the inner radius of the hollow particle is A, and the outer radius is B. The particle is coated by a stiff shell of outer radius C. Note that a typical value of lithium diffusivity in amorphous silicon is $\sim 10^{-16}$ m^2 s^{-1} [32,33], the diffusion time for lithium through a 100 nm silicon film can be estimated as on the order of 100 s ($t \sim L^2/D$). Such time is much shorter than the time of a lithiation

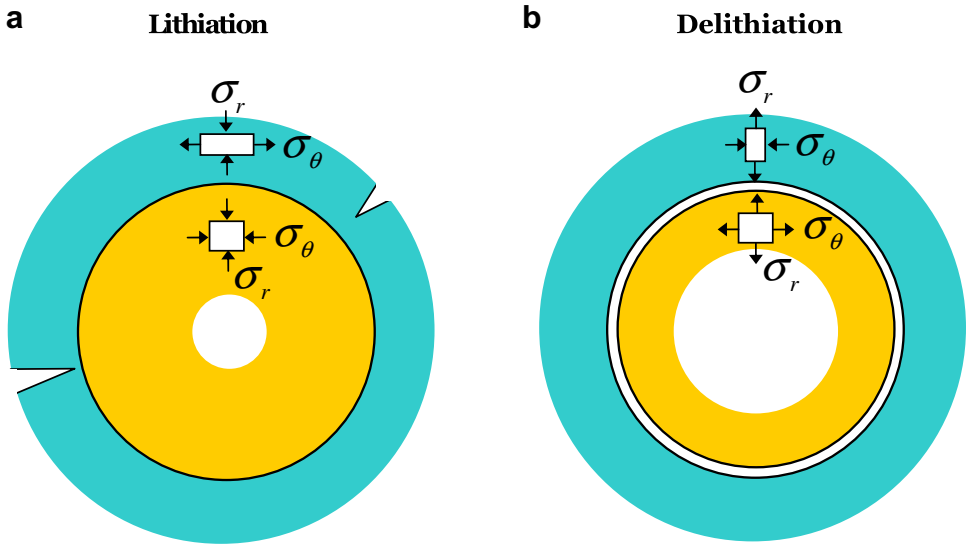

Fig. 2. Two potential modes of failure in a hollow silicon particle coated with a stiff shell. (a). The lithiation of the silicon particle induces tensile hoop stress in the shell, which may cause the shell to fracture. (b) The delithiation of the silicon particle induces radial tensile stress, which may cause debonding between the core and the shell.

cycle in typical electrochemical measurements. Thus we consider that diffusion in the core is fast to allow for a uniform distribution of lithium. To completely fill the hollow space upon full lithiation, the structure should satisfy the geometric relation:

$$\frac{A}{B} = \left(\frac{\beta - 1}{\beta}\right)^{1/3}, \tag{1}$$

where the volumetric swelling ratio $\beta = V_f/V_i$, with V_f representing the fully lithiated volume and V_i the initial volume of the lithium-free state. Lithiation of silicon causes a volumetric swelling $\beta = 4$, so that $A/B = (3/4)^{1/3}$. [34]

We take the stress-free and lithium-free state as the reference state, Fig. 3(a). At time t, the hollow particle absorbs some lithium, retaining its spherical symmetry. We assume that the outward expansion of the core is completely constrained by the stiff shell. Note that the elastic deformation of the shell, typically less than 1%, is much less than the lithiation-induced strain in the silicon core. With this assumption, lithiation changes only the inner radius a, and we neglect any deformation of the shell, Fig. 3(b). We represent a material element in the reference state by its distance R from the center. At time t, it moves to a place a distance r from the center. The function $r(R, t)$ specifies the kinematics of the deformation. Each material element in the hollow core is subject to a state of triaxial stresses, $(\sigma_r, \sigma_\theta, \sigma_\theta)$, where σ_r is the radial stress and σ_θ the hoop stress. The stresses are inhomogeneous, represented by functions $\sigma_r(r, t)$ and $\sigma_\theta(r, t)$. The balance of forces acting on a material element requires that

$$\frac{\partial \sigma_r(r,t)}{\partial r} + 2\frac{\sigma_r(r,t) - \sigma_\theta(r,t)}{r} = 0. \tag{2}$$

We adopt the commonly used idealization that plastic deformation is unaffected when a hydrostatic stress is superimposed. Furthermore, the yield strength of the lithiated silicon, σ_Y, is taken to be constant and independent of the amount of deformation and the concentration of lithium [35]. Because the elastic strain is negligible compared to the lithiation-induced strain, the elasticity of the hollow core is neglected. During lithiation, a material element of silicon is under compression in the hoop direction and is in the state $\sigma_r - \sigma_\theta = \sigma_Y$. Setting $\sigma_r - \sigma_\theta = \sigma_Y$ in Eq. (2) and integrating over r with the traction-free boundary condition, $\sigma_r(a, t) = 0$, the radial stress in the hollow core is given by

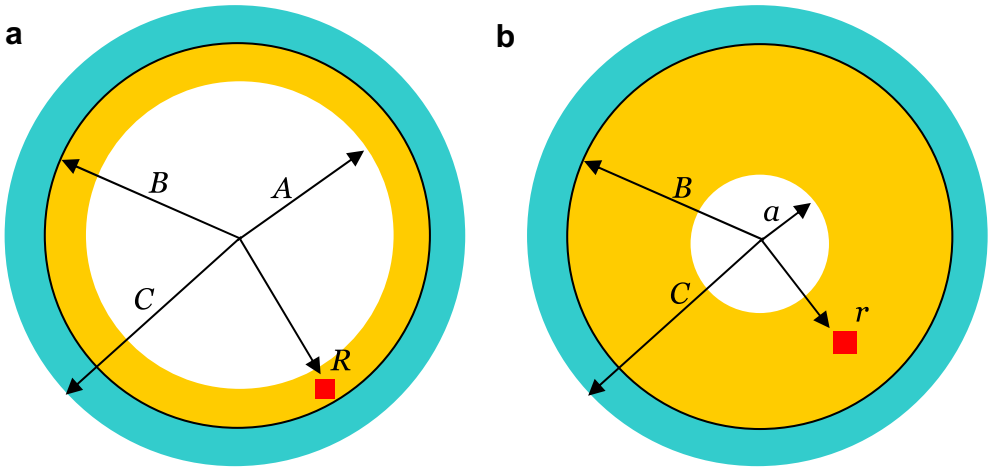

Fig. 3. (a). In the reference state, a hollow particle of an electrode is stress-free and lithium-free. (b) In the current state, the particle is partially lithiated. The deformation of the core is accommodated by the inner hollow space. Outward deformation is restricted by the shell.

$$\sigma_r = -2\sigma_Y \log\frac{r}{a}, \quad a \le r \le B. \tag{3}$$

The hoop stress in the hollow core is determined by $\sigma_r - \sigma_\theta = \sigma_Y$, giving

$$\sigma_\theta = -\sigma_Y\left(2\log\frac{r}{a} + 1\right), \quad a \le r \le B \tag{4}$$

The stress fields in the elastic shell take the familiar solutions of Lamé problems [36], with the radial stress

$$\sigma_r = -2\sigma_Y\left(\log\frac{B}{a}\right)\left(\frac{B^3}{C^3 - B^3}\right)\left(\frac{C^3}{r^3} - 1\right), \quad B < r \le C, \tag{5}$$

and the hoop stress

$$\sigma_\theta = 2\sigma_Y\left(\log\frac{B}{a}\right)\left(\frac{B^3}{C^3 - B^3}\right)\left(\frac{C^3}{2r^3} + 1\right), \quad B < r \le C \tag{6}$$

During delithiation, a material element of the hollow core is under tension in the hoop direction, and is in the state $\sigma_r - \sigma_\theta = -\sigma_Y$. Setting $\sigma_r - \sigma_\theta = -\sigma_Y$ in Eq. (2) we obtain the radial stress in the hollow core by integrating over r,

$$\sigma_r = 2\sigma_Y \log\frac{r}{a}, \quad a \le r \le B, \tag{7}$$

and the hoop stress,

$$\sigma_\theta = \sigma_Y\left(2\log\frac{r}{a} + 1\right), \quad a \le r < B \tag{8}$$

A comparison of the stress fields indicates a jump in both the radial and hoop stresses from lithiation to delithiation, as shown in Fig. (4). These jumps are caused by neglecting the elastic strain. Should we include the elastic strain, the stresses would make this transition from compressive to tensile yielding after the removal of a very small amount of lithium.

Mechanical failure is mainly due to the stress at the interface between the core and shell. Fig. 4 plots the evolution of the radial stress at the interface of the hollow core during lithiation and delithiation. The stress is plotted as a function of the state of charge (SOC) – 0 represents the lithium-free state, and 1 the fully lithiated state. Given the geometric condition in Eq. (1), the state of charge is calculated by using the inner radius a at a given state,

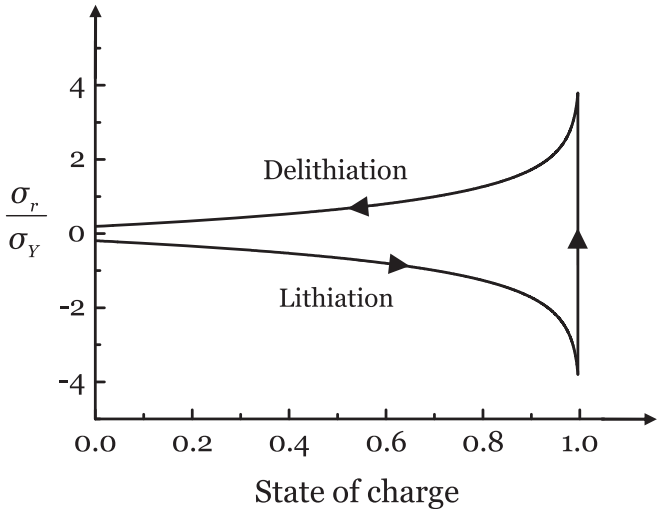

Fig. 4. Evolution of the radial stress at the interface between the particle and the shell during lithiation and delithiation.

$$\text{SOC} = \frac{A^3 - a^3}{A^3}. \tag{9}$$

As expected, the hollow core is under compression in the radial direction during lithiation. The compressive stress increases logarithmically with the state of lithiation, Eq. (3). Because of the triaxial state of stress, the magnitudes of the components of the stress readily exceed the yield strength of lithiated silicon [37]. Such big compressive stresses in the core can cause a large tensile hoop stress in the outer shell, which may lead to fracture of the shell. During delithiation, the core–shell interface is under tensile stress in both the radial and hoop directions. The magnitudes of the stress components are maximized at the beginning of the delithiation, and gradually decrease with the state of delithiation. The tensile stress in the radial direction may initiate interfacial debonding, resulting in a loss of electrical contact between the active core and the surface coating.

3. Fracture and debonding analysis

We now analyze fracture of the coating using an approach similar to that described in several recent papers [38–40]. We focus on fracture of the coating caused by the tensile hoop stress during lithiation. Linear elastic fracture mechanics are adopted. The reduction in the elastic energy associated with a crack advancing a unit area defines the energy release rate G_f. Dimensional analysis dictates that the energy release rate should take the form

$$G_f = Z\frac{\sigma_\theta^2}{E_s}(C - B). \tag{10}$$

where E_s is Young's modulus of the shell, Z a dimensionless parameter to be determined by solving the elastic boundary-value problem, σ_θ the stress in the hoop direction given by Eq. (6), and $C - B$ the thickness of the surface coating. In the case of a channel crack in the thin shell, $Z = 2$ is a typical value. Inserting this value of Z and Eq. (6) into Eq. (10) gives an analytical solution of the energy release rate

$$G_f = \frac{8\sigma_Y^2}{E_s}\left(\log\frac{B}{a}\right)^2\left(\frac{B^3}{C^3 - B^3}\right)^2\left(1 + \frac{C^3}{2B^3}\right)^2(C - B), \tag{11}$$

where we have approximated $r \approx B$ since $B >> C - B$. In this limit, Eq. (11) can be further approximated as

$$G_f \approx 2\frac{\sigma_Y^2}{E_s}\left(\log\frac{B}{a}\right)^2\frac{B^2}{C - B}. \tag{12}$$

The energy release rate is proportional to the square of the yield strength of lithiated silicon, the compliance of the surface coating, the ratio of the sizes of core and shell, and the size of the core. Therefore, to minimize the energy release rate, it is desired to have a small and soft hollow core and a thick and stiff surface shell. However, the shell also needs to be thin to minimize weight and to allow for fast diffusion of lithium through its thickness.

We take the same approach for the analysis of interfacial debonding. Debonding of thin-film electrodes from a substrate associated with lithiation cycles has been observed in experiments [41,42] and analyzed in theories [10,43]. Here we consider that the driving force of debonding, the energy release rate, is mainly attributed to mode I fracture caused by the tensile radial stress at the interface of the silicon core and the stiff shell. We assume a pre-existing crack of a size comparable to the thickness of the shell, $C - B$. The energy release rate may be reduced to a simple form,

$$G_d = \pi \frac{\sigma_r^2}{E_e}(C - B). \quad (13)$$

The value of the numerical pre-factor in (13) is approximate, which changes somewhat with the elastic mismatch between the shell and the core, and with the relative length of the crack to the thickness of the shell. Accurate values of the factor can be calculated by solving the boundary-value problem using the finite-element method [38]. In this work, however, a particular value is used to illustrate these main ideas. The radial stress during delithiation is given by Eq. (7), and thus

$$G_d = 4\pi \frac{\sigma_Y^2}{E_e}\left(\log\frac{B}{a}\right)^2 (C - B). \quad (14)$$

Here E_e is the effective modulus that accounts for the effects of inhomogeneous properties of the core and shell. A typical relation is represented by

$$\frac{1}{E_e} = \left(\frac{1}{E_c} + \frac{1}{E_s}\right)\Big/ 2, \quad (15)$$

where E_c is the modulus of the core, and E_s the modulus of the shell. [44] Comparing Eqs. (12) and (14), we can see some interesting differences. Namely, the energy release rate for interfacial debonding is seen to scale directly with the shell thickness while the energy release rate for fracture of the shell scales inversely with the shell thickness. Furthermore, the energy release rate for debonding scales much more slowly with the core radius B, than does the energy release rate for fracture of the shell.

Let Γ_f be the fracture energy of the shell, and Γ_d the interfacial energy between the core and the shell. No preexisting flaws will advance if the maximum energy release rate is less than the fracture energy. Therefore, $G_f = \Gamma_f$ defines the critical condition for initiation of fracture of the shell, and $G_d = \Gamma_d$ defines the critical condition for initiation of interfacial debonding.

Recent experiments indicate that a thin layer of Al_2O_3 deposited on silicon anodes by atomic layer deposition provides excellent improvement of the cycling stability of silicon anodes [17,21]. Here we take the example of a hollow spherical particle of silicon coated with a thin shell of Al_2O_3 to illustrate the above analysis. Representative values of lithiated silicon and Al_2O_3 are taken, $\sigma_Y = 1$ GPa [35] and $E_c = 12$ GPa for lithiated silicon [45,46], $E_s = 300$ GPa, $\Gamma_f = 40$ J m^{-2} [47], and $\Gamma_d = 1$ J m^{-2}.

We first construct a phase diagram to show the effects of the thickness of the shell and the state of charge, Fig. 5(a). We take a typical value of the silicon core size, $B = 200$ nm and $A/B = \sqrt[3]{3/4}$. The thickness of Al_2O_3, $C - B$, is varied. The state of charge is calculated from Eq. (9). The solid black line represents the critical conditions for fracture of the shell, corresponding to the condition $G_f = \Gamma_f$, and the red dashed line (in the web version) represents the critical conditions of interfacial debonding, corresponding to the condition $G_d = \Gamma_d$. These two lines delineate an upper boundary to the safe regime in which no fracture of the surface coating or interfacial debonding would occur. Fig. 5(b) further plots a phase diagram to show the effects of core size and state of charge. In this case, the thickness of the Al_2O_3 shell is fixed, $C - B = 5$ nm, and the core size B is varied while maintaining the geometric relation $A/B = \sqrt[3]{3/4}$. Given the analytical solutions in Eqs. (11) and (14), phase diagrams for other experimental conditions can be readily constructed.

4. Analysis of coated hollow silicon nanowires

One dimensional nanowires and nanotubes are emerging designs that can mitigate the mechanical failure of silicon electrodes. In particular, Y. Cui and co-workers illustrate that coated hollow nanowires enable silicon anodes to sustain over six thousands cycles with high coulombic efficiencies [28]. Such excellent performance would ultimately meet the requirement of commercializing silicon into electric vehicles. In this section, we analyze fracture and debonding of a hollow nanowire. The cross-section is as shown in Fig. 3. For complete utilization of the available hollow volume upon full lithiation, we must satisfy the geometric relation:

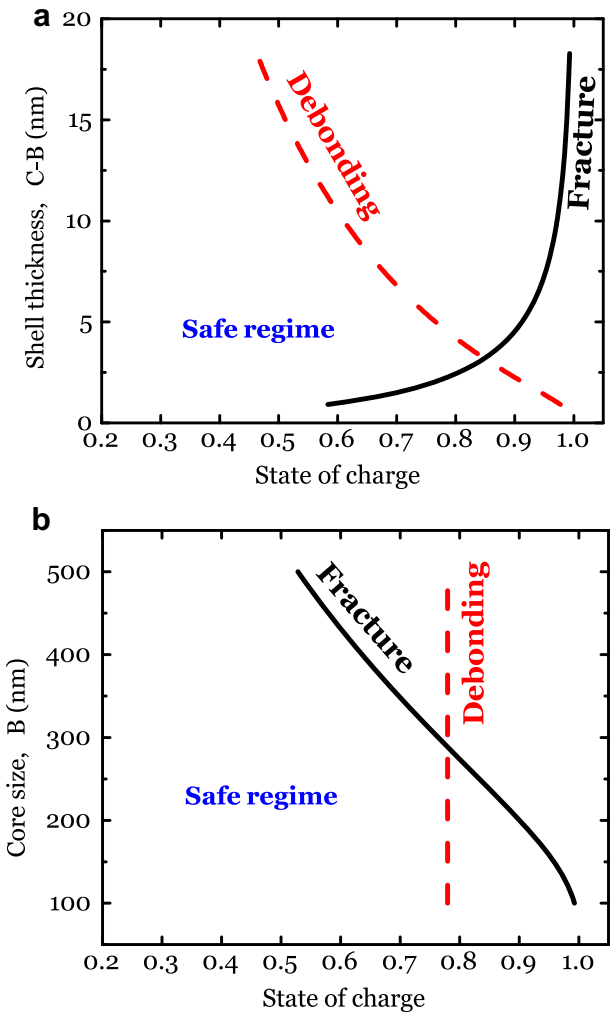

Fig. 5. Conditions of fracture and debonding for a spherical hollow particle plotted in the plane of (a) the thickness of the shell and the state of charge, and (b) the radius of the particle and the state of charge.

$$\frac{A}{B} = \left(\frac{\beta - 1}{\beta}\right)^{1/2}, \quad (16)$$

where for silicon $\beta = 4$ and $A/B = (3/4)^{1/2}$.

Similar to the case of spherical particles, lithiation of silicon causes a tensile hoop stress in the shell, which may fracture the coating material. Furthermore, a large tensile radial stress is developed at the beginning of delithiation, which may initiate interfacial debonding. We derive the stress field in the Appendix. Since the deformation of the core along the axial direction is constrained by the shell, lithiated silicon is assumed to deform under plane-strain conditions. The analytical solution of fracture energy release rate of the shell during lithiation is given by

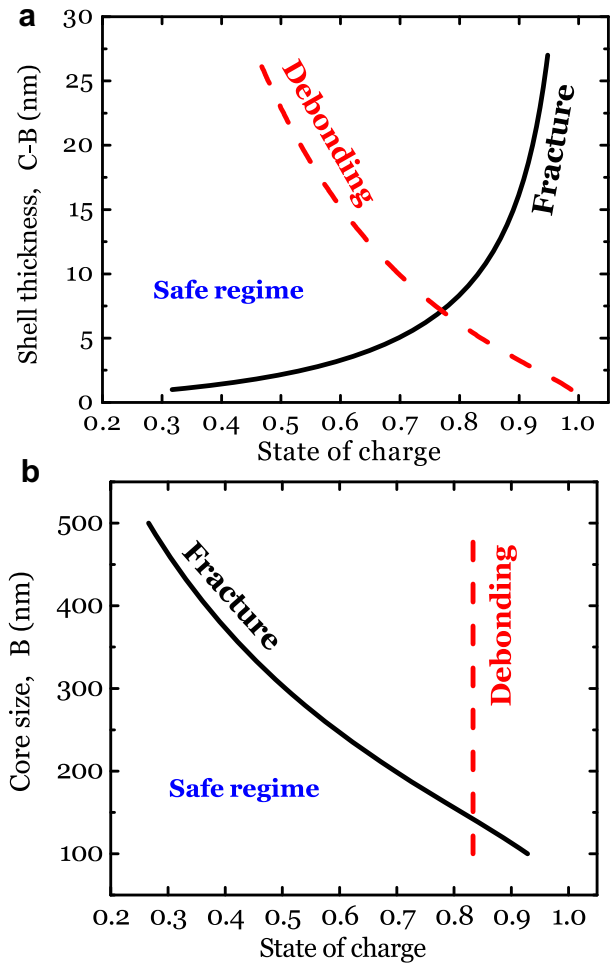

Fig. 6. Conditions of fracture and debonding for a hollow nanowire plotted in the plane of (a) the thickness of the shell and the state of charge, and (b) the radius of the particle and the state of charge.

$$G_f = \frac{8}{3}\frac{\sigma_Y^2}{E_s}\left(\log\frac{B}{a}\right)^2\left(\frac{B^2}{C^2-B^2}\right)^2\left(1+\frac{C^2}{B^2}\right)^2(C-B). \quad (17)$$

In the case of $C \approx B$, Eq. (17) can be further approximated as

$$G_f \approx \frac{8}{3}\frac{\sigma_Y^2}{E_s}\left(\log\frac{B}{a}\right)^2\frac{B^2}{C-B}. \quad (18)$$

And the interfacial fracture energy during delithiation is given by

$$G_d = \frac{4\pi}{3}\frac{\sigma_Y^2}{E_e}\left(\log\frac{B}{a}\right)^2(C-B) \quad (19)$$

Comparing the fracture energies in the spherical particle and the nanowire, we find that the energy release rate for fracture of the shell is a factor of 4/3 larger for the nanowire than for the sphere. In contrast, energy release rate for interfacial debonding is 3 times larger in the sphere than in the nanowire.

We now consider the practical example of a hollow silicon nanowire coated with a thin layer of Al_2O_3. A phase diagram showing the effects of the thickness of the shell and the state of charge is given in Fig. 6(a). In the nanowires, the state of charge is calculated by

$$\mathrm{SOC} = \frac{A^2-a^2}{A^2}. \quad (20)$$

The silicon core size is taken as $B = 200$ nm and $A/B = (3/4)^{1/2}$. The thickness of Al_2O_3, $C - B$, is varied. The solid black line corresponds to the critical conditions of fracture of the shell, given by $G_f = \Gamma_f$, and the red dashed line (in the web version) corresponds to the critical conditions for interfacial debonding, given by $G_d = \Gamma_d$. Fig. 6(b) shows a phase diagram demonstrating the effects of the core size and state of charge. In this case, the thickness of the Al_2O_3 shell is taken as $C - B = 5$ nm and the core size B is varied while maintaining the geometric relation $A/B = \sqrt{3/4}$. More accurate measurements of Γ_f and Γ_d are needed to produce more accurate plots. In the case where the fracture energies Γ_f and Γ_d are less than the values we have used here, the black and red dashed lines in Figs. (5) and (6) would shift to lower limits of the state of charge.

5. Stress effect on the lithiation reaction

We now identify the driving forces for the lithiation reaction of silicon, namely, the change of free energy associated with the reaction. Let ΔG_r be the free energy of the lithiation reaction of silicon when both the stress and the applied voltage vanish. Assume the silicon anode is connected to a cathode by a conducting wire through a voltage source. Associated with converting one lithium atom and silicon into lithiated silicon, one electron passes through the external wire, so that the voltage source does work $e\Phi$, where Φ is the voltage, and e the elementary charge (a positive quantity). The driving force is further modified when the stress effect is included. During lithiation of the coated hollow silicon particle, lithium atoms migrate into silicon by overcoming an energy barrier induced by the compressive stress in the core. Thus, when one lithium atom is incorporated into lithiated silicon, the stress does work $-\Omega\sigma_m$, where σ_m is the mean stress in the core, and Ω is the change in volume caused by insertion of one lithium atom. Here we assume an isotropic swelling of silicon caused by lithium insertion such that only the contribution from the mean stress is included. We also consider small elastic deformation of lithiated silicon such that stress terms of higher orders can be neglected [48,49]. Combining the above contributions, we find that, when the reaction advances, the net change in the free energy is

$$\Delta G = \Delta G_r - e\Phi - \Omega\sigma_m. \quad (21)$$

We have neglected the dissipation at the electrolyte/electrode interfaces, as well as inside the electrodes and electrolytes. In our sign convention, a negative ΔG drives lithiation, and a more negative value represents a larger driving force. The free energy of reaction ΔG_r takes a negative value. The sign of $e\Phi$ depends on the polarity. We consider Φ to be positive in the direction that drives lithiation. As expected, a compressive mean stress in silicon retards lithiation.

For both the spherical silicon particles and nanowires, the analytical solutions of the stress fields are given in the prior sections. Inserting the stresses into Eq. (21), we can quantify the effect of stress on the lithiation reaction. We note that the compressive stress is maximized at the core–shell interface. Thus, the retarding effect of stress on the lithiation reaction is most significant at the interface. The contribution due to the stresses at the interface is plotted in Fig. 7. In making this plot, we have adopted the value $\Omega = 1.36 \times 10^{-29}$ m^3 [50]. As expected, the magnitude of the stress contribution increases with the state of charge. Recall that the free energy of formation of lithiated silicon is small; for example, $\Delta G_r = -0.18$ eV for amorphous $Li_{2.1}Si$ [51]. Consequently, the reaction can readily generate a large enough stress to counteract the electrochemical driving force, stalling the

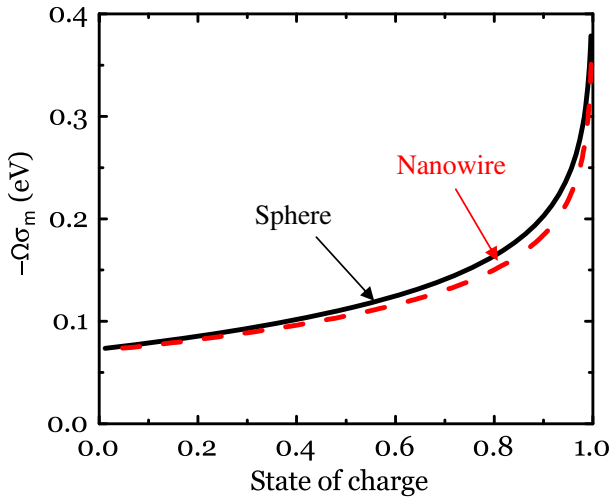

Fig. 7. The effect of the stress on the driving force for the lithiation reaction is plotted as a function of the state of charge.

surface reaction prior to complete lithiation. In fact, a lower lithiation capacity due to an incomplete surface reaction has been observed in recent experiments [15,52,53].

6. Conclusions

We present an analysis of fracture and debonding failure in coated hollow spherical particles and nanowires of silicon anodes. A phase diagram describing the critical structural parameters and operating conditions is constructed, outlining how to avoid fracture of the coating and debonding between the coating and the active material. We further explore the effect of the stress field on the lithiation reaction of silicon. The large compressive stress at the core–shell interface may counteract the electrochemical driving force, leading to a low lithiation capacity. The present results and associated analysis provide insightful guidelines for a viable design of coated hollow nanostructures.

Acknowledgments

This work is supported by the National Science Foundation through a grant on lithium-ion batteries (CMMI-1031161). MP acknowledges government support under and awarded by DoD, Air Force Office of Scientific Research, National Defense Science and Engineering Graduate (NDSEG) Fellowship, 32 CFR 168a.

Appendix

We derive the stress field in a hollow silicon nanowire coated with a stiff shell. The geometry of the cross section is represented in Fig. 3. We represent a material element in the reference configuration, Fig. 3(a), by its distance R from the center. At time t, it moves to a place at a distance r from the center, Fig. 3(b). The function $r(R, t)$ specifies the deformation kinematics of the silicon nanowire. Due to the constraint imposed by the shell, lithiated silicon is assumed to deform under the plane-strain conditions. To focus on the main ideas, we neglect the elasticity of both the core and the shell; we model the lithiated silicon as a rigid-plastic material. Consequently, the expansion of lithiated silicon is entirely due to lithiation. Consider an annulus of the lithiated silicon between the radii B and r. This annulus is lithiated from the annulus of pristine silicon between the radii B and R. We assume that the rate of lithiation is slow relative to diffusion of lithium in the core, so that lithium atoms have enough time to homogenize in the core. That is, the ratio of the volume of the lithiated silicon over the volume of pristine silicon $\tilde{\beta}$, is taken to be homogeneous and evolves in time. Upon full lithiation, $\tilde{\beta}$ reaches $\beta = 4$ for silicon. Thus,

$$B^2 - r^2 = \tilde{\beta}\left(B^2 - R^2\right), \tag{A.1}$$

This equation gives the function $r(R, t)$ once the function $\tilde{\beta}(t)$ is given. That is, $\tilde{\beta}(t)$ fully specifies the kinematics of the silicon nanowire,

$$r = \sqrt{B^2 - \tilde{\beta}\left(B^2 - R^2\right)}. \tag{A.2}$$

The stretches can be calculated as

$$\lambda_r = \frac{\partial r}{\partial R} = \frac{R\tilde{\beta}}{r}, \quad \lambda_\theta = \frac{r}{R}, \quad \lambda_z = 1, \tag{A.3}$$

We decompose the stretches by writing

$$\lambda_r = \lambda_r^p \tilde{\beta}^{1/3}, \quad \lambda_\theta = \lambda_\theta^p \tilde{\beta}^{1/3}, \quad \lambda_z = \lambda_z^p \tilde{\beta}^{1/3} \tag{A.4}$$

where $\tilde{\beta}$ represents the volume change due to the insertion of lithium, and the plastic stretch λ^p represents the shape change during lithiation. The volume change has been assumed to be isotropic for amorphous silicon. We can calculate the strain components from the stretches,

$$\varepsilon_r = \log\lambda_r, \quad \varepsilon_\theta = \log\lambda_\theta, \quad \varepsilon_z = \log\lambda_z \tag{A.5}$$

The incremental plastic deformation is given by

$$\begin{aligned}
\delta\varepsilon_r^p &= \delta\log\lambda_r - \frac{1}{3}\delta\log\tilde{\beta} = \left(\frac{1}{6} + \frac{1}{2}\frac{B^2}{r^2}\right)\frac{\delta\tilde{\beta}}{\tilde{\beta}},\\
\delta\varepsilon_\theta^p &= \delta\log\lambda_\theta - \frac{1}{3}\delta\log\tilde{\beta} = \left(\frac{1}{6} - \frac{1}{2}\frac{B^2}{r^2}\right)\frac{\delta\tilde{\beta}}{\tilde{\beta}},\\
\delta\varepsilon_z^p &= \delta\log\lambda_z - \frac{1}{3}\delta\log\tilde{\beta} = -\frac{1}{3}\frac{\delta\tilde{\beta}}{\tilde{\beta}}.
\end{aligned} \tag{A.6}$$

The equivalent plastic strain is

$$\delta\varepsilon_{eq}^p = \sqrt{\frac{2}{3}\delta\varepsilon_{ij}^p\delta\varepsilon_{ij}^p} = \frac{\delta\tilde{\beta}}{\tilde{\beta}}\sqrt{\frac{1}{9} + \frac{1}{3}\frac{B^4}{r^4}}. \tag{A.7}$$

We adopt the flow rule

$$s_{ij} = \frac{2}{3}\frac{\sigma_Y}{\delta\varepsilon_{eq}^p}\delta\varepsilon_{ij}^p, \tag{A.8}$$

where s_{ij} is the deviatoric stress, defined as $s_{ij} = \sigma_{ij} - (1/3)\sigma_{ij}\delta_{ij}$, and σ_Y the yield strength of lithiated silicon. Therefore,

$$\begin{aligned}
s_r &= \frac{\sigma_Y}{\sqrt{\frac{1}{9} + \frac{1}{3}\frac{B^4}{r^4}}}\left(\frac{1}{9} + \frac{1}{3}\frac{B^2}{r^2}\right),\\
s_\theta &= \frac{\sigma_Y}{\sqrt{\frac{1}{9} + \frac{1}{3}\frac{B^4}{r^4}}}\left(\frac{1}{9} - \frac{1}{3}\frac{B^2}{r^2}\right),\\
s_z &= -\frac{2}{9}\frac{\sigma_Y}{\sqrt{\frac{1}{9} + \frac{1}{3}\frac{B^4}{r^4}}},
\end{aligned} \tag{A.9}$$

and

$$\sigma_r - \sigma_\theta = s_r - s_\theta = \frac{2\sigma_Y}{\sqrt{r^4/B^4+3}}. \quad (A.10)$$

Consider the force balance of a material element in lithiated silicon

$$\frac{\partial \sigma_r}{\partial r} + \frac{\sigma_r - \sigma_\theta}{r} = 0, \quad (A.11)$$

the radial stress can be obtained by integrating Eq. (A.11), it gives

$$\sigma_r = -\frac{\sqrt{3}}{3}\sigma_Y \log\frac{\sqrt{r^4+3B^4}-\sqrt{3}B^2}{r^2} + D, \quad a \le r \le B \quad (A.12)$$

where D is the integration constant. With the traction-free boundary condition, $\sigma_r(a, t) = 0$,

$$\sigma_r = -\frac{\sqrt{3}}{3}\sigma_Y\left(2\log\frac{a}{r} + \log\frac{\sqrt{r^4+3B^4}-\sqrt{3}B^2}{\sqrt{a^4+3B^4}-\sqrt{3}B^2}\right), \quad a \le r \le B \quad (A.13)$$

The stresses along hoop and axial directions are obtained from Eqs. (A.9) and (A.10),

$$\begin{aligned}\sigma_\theta &= \sigma_r - \frac{2\sigma_Y}{\sqrt{r^4/B^4+3}} \\ \sigma_z &= \sigma_r - \frac{\sigma_Y}{\sqrt{r^4/B^4+3}} - \frac{\sigma_Y}{\sqrt{3B^4/r^4+1}},\end{aligned} \quad (A.14)$$

Therefore the radial stress at the interface $r = B$ is given by,

$$\sigma_r = -\frac{\sqrt{3}}{3}\sigma_Y\left(2\log\frac{a}{B} + \log\frac{\left(2-\sqrt{3}\right)B^2}{\sqrt{a^4+3B^4}-\sqrt{3}B^2}\right). \quad (A.15)$$

In the fully lithiated state of a hollow silicon nanowire, $a << B$. The radial stress at the interface can then be approximated by a Taylor expansion, which gives

$$\sigma_r \approx \frac{2\sqrt{3}}{3}\sigma_Y \log\frac{a}{B}. \quad (A.16)$$

The stress field in the elastic shell can be solved using the familiar solution of Lamé problem [36], it gives,

$$\begin{aligned}\sigma_r &= -\frac{2\sqrt{3}}{3}\sigma_Y\left(\log\frac{a}{B}\right)\left(\frac{B^2}{C^2-B^2}\right)\left(1-\frac{C^2}{r^2}\right), \\ \sigma_\theta &= -\frac{2\sqrt{3}}{3}\sigma_Y\left(\log\frac{a}{B}\right)\left(\frac{B^2}{C^2-B^2}\right)\left(1+\frac{C^2}{r^2}\right), \quad B < r \le C \\ \sigma_z &= -\frac{2\sqrt{3}}{3}\sigma_Y\left(\log\frac{a}{B}\right)\left(\frac{2\nu B^2}{C^2-B^2}\right).\end{aligned} \quad (A.17)$$

Similar to the analysis of a sphere, the energy release rate in the coating shell takes the following solution

$$G_f = \frac{8}{3}\frac{\sigma_Y^2}{E_s}\left(\log\frac{B}{a}\right)^2\left(\frac{B^2}{C^2-B^2}\right)^2\left(1+\frac{C^2}{B^2}\right)^2(C-B). \quad (A.18)$$

During delithiation, the tensile radial stress in silicon at the interface becomes

$$\sigma_r \approx \frac{2\sqrt{3}}{3}\sigma_Y \log\frac{B}{a}. \quad (A.19)$$

Thus, using Eq. (14), the energy release rate for interfacial debonding takes the solution

$$G_d = \frac{4\pi}{3}\frac{\sigma_Y^2}{E_e}\left(\log\frac{B}{a}\right)^2(C-B) \quad (A.20)$$

References

[1] M.S. Whittingham, Mrs Bull. 33 (2008) 411.
[2] M. Armand, J.M. Tarascon, Nature 451 (2008) 652.
[3] U. Kasavajjula, C.S. Wang, A.J. Appleby, J. Power Sources 163 (2007) 1003.
[4] W.J. Zhang, J. Power Sources 196 (2011) 13.
[5] N.S. Choi, Y. Yao, Y. Cui, J. Cho, J. Mater. Chem. 21 (2011) 9825.
[6] R.A. Huggins, W.D. Nix, Ionics 6 (2000) 57.
[7] B.J. Dimitrijevic, K.E. Aifantis, K. Hackl, J. Power Sources 206 (2012) 343.
[8] C.K. Chan, H.L. Peng, G. Liu, K. McIlwrath, X.F. Zhang, R.A. Huggins, Y. Cui, Nat. Nanotechnol. 3 (2008) 31.
[9] T. Takamura, S. Ohara, M. Uehara, J. Suzuki, K. Sekine, J. Power Sources 129 (2004) 96.
[10] H. Haftbaradaran, X. Xiao, M.W. Verbrugge, H. Gao, J. Power Sources 206 (2012) 357.
[11] C. Yu, X. Li, T. Ma, J. Rong, R. Zhang, J. Shaffer, Y. An, Q. Liu, B. Wei, H. Jiang, Adv. Mater. 2 (2012) 68.
[12] S.K. Soni, B.W. Sheldon, X. Xiao, M.W. Verbrugge, D. Ahn, H. Haftbaradaran, H. Gao, J. Electrochem. Soc. 159 (2012) A38.
[13] Y. Yao, M.T. McDowell, I. Ryu, H. Wu, N.A. Liu, L.B. Hu, W.D. Nix, Y. Cui, Nano Lett. 11 (2011) 2949.
[14] H. Kim, B. Han, J. Choo, J. Cho, Angew. Chem. Int. Ed. 47 (2008) 10151.
[15] M.T. McDowell, S.W. Lee, I. Ryu, H. Wu, W.D. Nix, J.W. Choi, Y. Cui, Nano Lett. 11 (2011) 4018.
[16] B. Hertzberg, A. Alexeev, G. Yushin, J. Am. Chem. Soc. 132 (2010) 8548.
[17] X.C. Xiao, P. Lu, D. Ahn, Adv. Mater. 23 (2011) 3911.
[18] H.X. Chen, Y. Xiao, L. Wang, Y. Yang, J. Power Sources 196 (2011) 6657.
[19] Y. Liu, N.S. Hudak, D.L. Huber, S.J. Limmer, J.P. Sullivan, J.Y. Huang, Nano Lett. 11 (2011) 4188.
[20] Y. He, X. Yu, Y. Wang, H. Li, X. Huang, Adv. Mater. 23 (2011) 4938.
[21] K. Leung, Y. Qi, K.R. Zavadil, Y.S. Jung, A.C. Dillon, A.S. Cavanagh, S.H. Lee, S.M. George, J. Am. Chem. Soc. 133 (2011) 14741.
[22] N.S. Choi, K.H. Yew, K.Y. Lee, M. Sung, H. Kim, S.S. Kim, J. Power Sources 161 (2006) 1254.
[23] Y.S. Hu, R. Demir-Cakan, M.M. Titirici, J.O. Muller, R. Schlogl, M. Antonietti, J. Maier, Angew. Chem. Int. Ed. 47 (2008) 1645.
[24] C.K. Chan, R. Ruffo, S.S. Hong, Y. Cui, J. Power Sources 189 (2009) 1132.
[25] M. Holzapfel, H. Buqa, W. Scheifele, P. Novak, F.M. Petrat, Chem. Commun. 12 (2005) 1566.
[26] M. Holzapfel, H. Buqa, F. Krumeich, P. Novak, F.M. Petrat, C. Veit, Electrochem. Solid State Lett. 8 (2005) A516.
[27] M. Ulldemolins, F.L. Cras, B. Pecquenard, V.P. Phan, L. Martin, H. Martinez, J. Power Sources 206 (2012) 245.
[28] H. Wu, G. Chan, J.W. Choi, I. Ryu, Y. Yao, M.T. McDowell, S.W. Lee, A. Jackson, Y. Yang, L. Hu, Y. Cui, Nat. Nanotechnol. (2012). http://dx.doi.org/10.1038/NNANO.2012.35.
[29] H. Wu, G. Zheng, N. Liu, T.J. Carney, Y. Yang, Y. Cui, Nano Lett. 12 (2012) 904.
[30] T.H. Hwang, Y.M. Lee, B. Kong, J. Seo, J.W. Choi, Nano Lett. 12 (2012) 802.
[31] X. Li, P. Meduri, X. Chen, W. Qi, M.H. Engelhard, W. Xu, F. Ding, J. Xiao, W. Wang, C. Wang, J. Zhang, J. Liu, J. Mater. Chem. (2012). http://dx.doi.org/10.1039/c0xx00000x.
[32] N. Ding, J. Xu, Y.X. Yao, G. Wegner, X. Fang, C.H. Chen, I. Lieberwirth, Solid State Ionics 180 (2009) 222.
[33] J. Xie, N. Imanishi, T. Zhang, A. Hirano, Y. Takeda, O. Yamamoto, Mater. Chem. Phys. 120 (2010) 421.
[34] L.Y. Beaulieu, K.W. Eberman, R.L. Turner, L.J. Krause, J.R. Dahn, Electrochem. Solid State Lett. 4 (2001) A137.
[35] V.A. Sethuraman, M.J. Chon, M. Shimshak, V. Srinivasan, P.R. Guduru, J. Power Sources 195 (2010) 5062.
[36] S. Timoshenko, J.N. Goodier, Theory of Elasticity, third ed, Mcgraw-Hill College, Blacklick, OH, 1970.
[37] K.J. Zhao, M. Pharr, S.Q. Cai, J.J. Vlassak, Z.G. Suo, J. Am. Ceram. Soc. 94 (2011) S226.
[38] K.J. Zhao, M. Pharr, J.J. Vlassak, Z.G. Suo, J. Appl. Phys. 108 (2010) 073517.
[39] K.J. Zhao, M. Pharr, J.J. Vlassak, Z.G. Suo, J. Appl. Phys. 109 (2011) 016110.
[40] W.H. Woodford, Y.-M. Chiang, W.C. Carter, J. Electrochem. Soc. 157 (2010) A1052.
[41] M. Winter, J.O. Besenhard, Electrochim. Acta 45 (1999) 31.
[42] J.P. Maranchi, A.F. Hepp, A.G. Evans, N.T. Nuhfer, P.N. Kumta, J. Electrochem. Soc. 153 (2006) A1246.
[43] F. Yang, J. Power Sources 196 (2011) 465.
[44] J.W. Hutchinson, Z. Suo, Adv. Appl. Mech. 29 (1991) 63.
[45] B. Hertzberg, J. Benson, G. Yushin, Electrochem. Commun. 13 (2011) 818.

[46] V.A. Sethuraman, M.J. Chon, M. Shimshak, N. Van Winkle, P.R. Guduru, Electrochem. Commun. 12 (2010) 1614.
[47] http://accuratus.com/alumox.html.
[48] Z. Cui, F. Gao, J. Qu, J. Mech. Phys. Solids (2012). http://dx.doi.org/10.1016/j.jmps.2012.03.008.
[49] V.A. Sethuraman, V. Srinivasan, A.F. Bower, P.R. Guduru, J. Electrochem. Soc. 11 (2010) A1253.
[50] K.J. Zhao, W.L. Wang, J. Gregoire, M. Pharr, Z.G. Suo, J.J. Vlassak, E. Kaxiras, Nano Lett. 11 (2011) 2962.
[51] P. Limthongkul, Y.I. Jang, N.J. Dudney, Y.M. Chiang, Acta Mater. 51 (2003) 1103.
[52] H. Haftbaradaran, H.J. Gao, W.A. Curtin, Appl. Phys. Lett. 96 (2010) 091909.
[53] S. Xun, X. Song, L. Wang, M.E. Grass, Z. Liu, V.S. Battaglia, G. Liu, J. Electrochem. Soc. 158 (2011) A1260.